2008 IEEE International Conference on
Robotics and Automation
Pasadena, CA, USA, May 19-23, 2008

12D Force and Acceleration Sensing: A Helpful Experience Report on Sensor Characteristics

Torsten Kröger, Daniel Kubus, and Friedrich M. Wahl
Institute for Robotics and Process Control
Technical University of Braunschweig, Germany
{t.kroeger, d.kubus, f.wahl}@tu-bs.de

***Abstract*—The potential of six-axis acceleration sensors in the field of robotic manipulation applications is quite high and most of it has not been used yet – neither in theoretic literature nor in research experiments. When considering six-joint industrial manipulators with six-axis force/torque and six-axis acceleration sensing, many new possibilities arise: all ten inertial parameters of any object can be identified and objects can be recognized based on these parameters, position control behavior can be improved; non-contact forces can be extracted and force control performance can be improved; visual-servoing methods can use acceleration signals to become more robust. The authors made numerous experiments in the mentioned fields and recognized major weaknesses during the realization of prototypic research setups with six-axis acceleration sensors. These problems regard sensor drift, undesired sensor-internal dependencies as the influence of any distal sensor part, noise, and undesired crosstalk behavior. In order to benefit from acceleration signals, it is important to clearly overcome these problems. This paper analyzes typical systematic errors, characterizes them, and suggests important solution methods for a successful usage of acceleration information.**

I. Introduction

Multi-sensor integration in industrial manipulation control systems provides a huge potential, of which only a very small part has been investigated yet. Industrial manipulators are still mainly used for point-to-point operations, i.e. purely position controlled. Commercial control units are not open for sensor integration, and research institutions often replace the existing control units by their own ones to perform experiments in control engineering and sensor integration.

This paper focuses on a very particular and important part of multi-sensor integration and multi-sensor fusion in order to improve the control of six-joint robotic manipulation arms: six-degree-of-freedom (DOF) force/torque sensing in combination with six-DOF acceleration sensing. Although six-axis accelerometers are commercially available since more than a decade, almost no results using this promising technology can be found in the open literature. Parts of the question *"Why?"* may also be answered by this paper.

The possibilities and advantages of this technique are wide spread; only some of the major operational areas and chances of it are supposed to be named in the following in order to emphasize its importance and potential. Identification of all ten inertial parameters (mass, center of mass coordinates, and the six elements of the inertia matrix) of a load attached to a manipulator by using the twelve sensor signals becomes possible and can be beneficially employed in various robotics applications. These parameters can be used to tune position controllers on-line. Especially when eying on parallel kinematic machines and their typical dynamic characteristics, the control behavior can be improved when not only the mass of the end-effector load is known but also its mass distribution given by the identified inertia tensor. The ten inertial parameters together with the six measured acceleration signals would also enable force controllers to extract the forces and torques caused by environmental contact(s) [1]. A new idea would be to use the ten parameters to identify objects [2]; this way even objects, which can not be distinguished by vision systems, can now be recognized, e.g. when handling castings with blowholes or crates of water: a vision system is not capable of detecting the trapped air, but by the knowledge of the inertial parameters this would become possible, too. The last application field to be mentioned here yields to a benefit in visual servoing. The approach presented in [3] applies position vision fusion for object tracking by using a Kalman filter. This approach might be extended by integrating the acceleration signals.

The authors made various experiments in the above mentioned fields and recognized that especially the characteristics of (six-DOF) accelerometer signals (still) do not satisfy the demands for a reasonable sensor fusion with force/torque signals. The reasons and proves for this statement together with suggestions to bypass this problem are given in this paper. A major aim is to prevent other researchers from making the same shortcoming experiences.

After related work and a brief introduction to six-DOF accelerometers are presented in Section II, Section III explains several reasons for the shortcoming of six-axis acceleration sensing, which is followed by a Section that describes how a six-tuple of acceleration values can alternatively be derived from position signals (Section IV). Experimental results are also presented in this Section, which is then followed by conclusions and references.

II. Related Work and Functional Principles of Six-Axis Accelerometers

Research on acceleration sensing has gained in popularity during the last years, but even up to now, literature on

acceleration sensing for robot control applications is rare. The moste relevant works in this field as well as corresponding (basic) functional principles are given in this Section.

Johansson et al. published works on the *estimation* of contact forces [4], [5]. There an observer, which is fed with position, force, and acceleration signals, is used to estimate the contact force. The respective theory includes Kalman filtering and leads to benefits in force/pose control, which was demonstrated with convincing experimental results. The authors of this work have worked on the *calculation* of contact forces and torques [1], [6]. Calculation means here, that the complete set of inertial parameters is known, and the acceleration signals are used to calculate (not to estimate) non-contact forces and torques in order subtract these values from the measured forces and torques, i.e.the measured force/torque six-tuple is divided into two parts: forces/torques caused by environmental contacts and forces/torques caused by inertia. Current activities include the on-line identification of all ten inertial parameters. The works of Meng et al. constitute research on six-axis accelerometers, which base on strain gages [7], [8], where special attention has been payed on robotic manipulation applications.

Several functional principles of six-axis accelerometers are known and supposed to be shortly introduced here. Acceleration sensing technologies base on *capacitive* (e.g. [9]), *piezoresistive* (e.g. [10]), *piezoelectric* (e.g. [11]), and other principles as the usage of strain gages with seismic masses by Meng et al. [7], [8] or the usage of optical distance sensors to measure to motion of a single proof mass [12].

Although some of these sensor technologies are already commercially available, their further enhancements are matter of research and development [10]. Due to recent advances in micromachining technology the fabrication and the design of MEMS-based (*micro-electromechanical-systems*) accelerometers has become more affordable and their characteristics as bandwidth, drift, temperature dependency, and sensitivity have been improved, too. A state-of-the-art report on MEMS, which are also used in [10] and [12], is given in [13].

One possibility to establish a minimal custom setup for twelve-DOF sensing is using any six-DOF force sensor in combination with a set of MEMS as shown in Fig. 1. Here three pairs of MEMS are arranged in angles of 120° on a cylindrical adapter part, which is supposed to be mounted between the manipulator's hand and the end-effector tool. Each pair measures in two orthogonal directions, such that acceleration values for all six DOFs can be extracted. As also shown in [14], special attention has to be payed to dynamic coupling effects between all sensors.

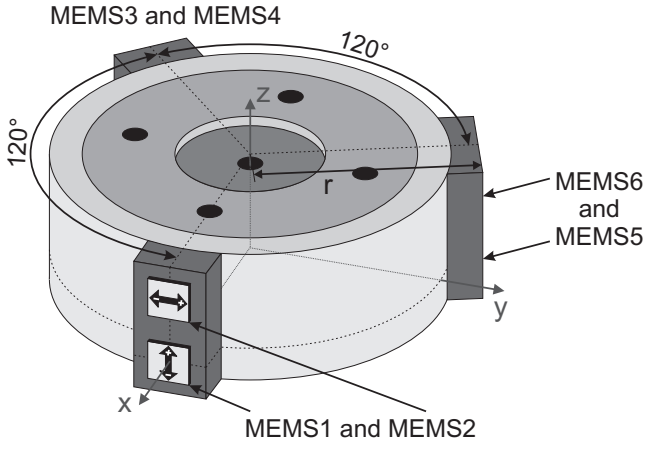

Fig. 1. Accelerometer for six DOFs based on three pairs of MEMS.

Considering the measured accelerations from MEMS1 to MEMS6 in Fig. 1 as $a_1, \ldots, a_6$, where a_1, a_3, and a_5 lay collinear to the sensor frame's z-axis and a_2, a_4, and a_6 are orientated tangentially with respect to the cylindrical adapter part at a radius of r, we can obtain the acceleration values in Euclidian space, a_x, a_y, a_z, α_x, α_y, and α_z, by:

$$a_x = \frac{a_6 - a_4}{\sqrt{3}} \quad (1) \qquad \alpha_x = \frac{a_5 - a_3}{\sqrt{3}\ r} \quad (4)$$

$$a_y = \frac{a_2 - 2a_4 - 2a_6}{3} \quad (2) \qquad \alpha_y = \frac{2a_3 + 2a_5 - a_1}{3r} \quad (5)$$

$$a_z = \frac{a_1 + a_3 + a_5}{3} \quad (3) \qquad \alpha_z = \frac{a_2 + a_4 + a_6}{3r} \quad (6)$$

This *geometric arrangement* of acceleration sensors was also chosen for the JR3 twelve-DOF combined force/torque and acceleration sensor [15], which provides six-DOF force/torque data and six-DOF acceleration data at a maximum sampling rate of $8\,kSamples/s$. This is a very convenient way to achieve all twelve desired signals, and as it is used by many research institutions, the focus will be put on this kind of sensor type in the following parts. But even if all concrete results described here are surely limited to this sensor type, the effects that have to be considered for twelve-DOF sensing are the same for any sensor. The authors achieved the here-presented results with a set of *85M35A-40 200N12* JR3 sensors[1], which are typical for robotic applications.

The analog outputs of the individual force, torque, and acceleration sensing elements are A/D converted within the sensor and transmitted to a receiver board. The receiver card performs processing tasks, e.g. decoupling of the sensor axes, optional low-pass filtering, and user-parameterizable functions. Forces and torques are sensed using foil strain gages, which show substantial drift due to temperature effects. Linear and angular acceleration values originate from a set of monolithic micro-machined accelerometers. This technique suggests that the noise affecting the linear and the angular accelerations may be correlated.

III. Systematic Errors

Various influences lead to errors in the measurement of forces, torques, and accelerations. This Section discusses systematic errors in the measurements and their causes, namely: sensor drift, the dependency on mounting torque, the influence of the distal sensor part, and issues concerning the impulse

[1]The maximum scale values of the sensor model *85M35A-40 200N12* are: $F_x = F_y = 200\,N$, $F_z = 400\,N$, $\tau_x = \tau_y = \tau_z = 12\,Nm$, $a_x = a_y = a_z = 49.03\,m/s^2$, $\alpha_x = \alpha_y = \alpha_z = 5729.58^\circ/s^2$.

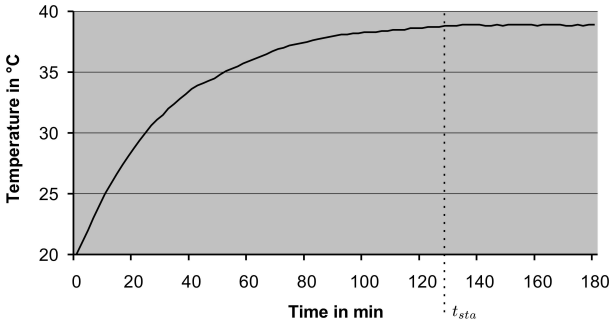

Fig. 2. Temperature evolution of the sensor surface during normal operation.

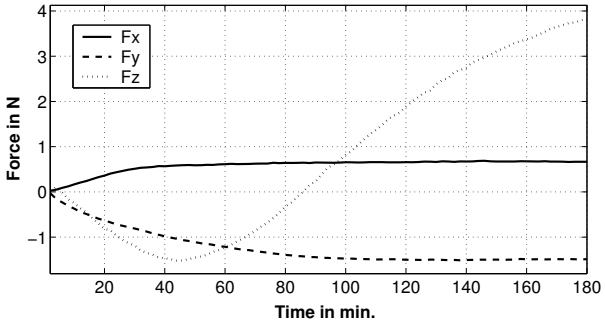

Fig. 3. Exemplary drift behavior of the three force offsets F_x, F_y, and F_z.

response. Finally some remarks on the noise characteristics are given.

A. Drift

The measured signals of the sample sensors exhibit noticeable offset drift, which abates after an operating time of approx. two hours, and which is not compensable. In order to quantify this observation and to evaluate the relation of the drift to the sensor temperature (self heating-up), the sensor *surface* temperature was monitored, and the evolution of all measured signals was observed simultaneously. As Fig. 2 shows, the temperature characteristics are of classical first-order time-delay behavior. Fig. 3 presents exemplarily the evolution of the force offsets over time. As can be observed in the figure, the changes of the offsets are not limited to $t < t_{sta}$ regarding all measured signals. The f_z signal shows the highest drift of more than $5\,N$. In contrast to the drift behavior of f_x and f_y, the drift of f_z does not considerably reduce after t_{sta}. In fact f_z is the only measured signal that shows considerable drift ($\approx\ 2\,N/h$) after the stabilization of the sensor surface temperature (cf. Fig. 2). Moreover the remaining force offsets were observed to show a noticeable drift ($<\ 0.3\,N/h$) even after twelve hours of operation at a constant sensor surface temperature. Similarly, the drift of the torque signals did not abate entirely. Regarding the remaining measured signals – i.e. the linear accelerations and the angular accelerations – a stabilization of the offsets is observed by t_{sta}. Apart from the heating-up of the sensor during operation, other temperature influences may result in offset drift. Noticeable fluctuations are caused by test-loads

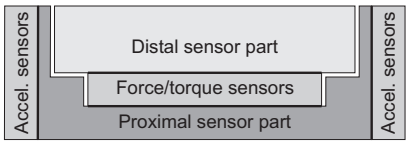

Fig. 4. Strongly simplified scheme of the sensor setup: the mass of the *distal sensor part* also influences sensor signals.

whose temperature differs from the sensor surface temperature. Therefore it is recommended to mount the test-load before the heating-up phase of the sensor, if stable sensor offsets are desired.

Summarizing this Subsection, users can only neglect this drift after a heating-up phase. The drift of the sensor in z-direction does not stop, might remain at $2\,N/h$, and cannot be neglected.

B. Mounting Torque Dependency

Mounting a load onto the sensor causes measured forces and torques that substantially differ from the expected gravitational forces and torques. This difference obviously depends on the torquing of the load. If the load is removed again, the force/torque readings approximately reduce to zero again. This observation indicates that the distal sensor part, i.e. the part of the sensor which is located between the sensing elements and the attached load, is elastically deformed by mounting (torquing) the load, which induces forces and torques into the strain gages. In order to quantify this observation, the forces/torques were measured before and after mounting an end-effector tool. The mounting bolts were torqued according to the scheme proposed in [15] with torques of $0.5\,Nm$, $1\,Nm$, and $1.5\,Nm$ in three experiments. Permanent forces of up to 22% of the full scale and torques of up to 25% were observed if the highest torque was applied. After removing the bolts the residual forces and torques reduce to values below or slightly above the noise level, i.e. $\vec{f}_{before} - \vec{f}_{after} < 0.04\,N$. These offset shifts occur regardless of whether the bolts are tightened with torques of $0.5\,Nm$, $1\,Nm$ or $1.5\,Nm$. Nevertheless the magnitude of these force and torque offsets rises with increasing mounting torque. As the force and torque offset shifts of these magnitudes can definitely not be neglected, zeroing becomes necessary after every change of mounting torques.

C. Influence of the Distal Sensor Part

Fig. 4 shows a very simplified scheme of the respective sensor device. The distal sensor part influences the force/torque readings depending on the orientation of the sensor. Despite the elastic properties and limited stiffness, the distal sensor part is *assumed to be a rigid body here*. If properly attached to the load, the distal part of the sensor and the load form *one* rigid body, that exerts forces and torques onto the sensor. The inertial parameters of the load are adulterated by the forces and torques caused by the distal sensor part. In order to compensate these forces and torques, the law of linear superposition of forces and torques should be applied. If the

ten inertial parameters of the distal sensor part are known, identification methods can be used to calculate the resulting forces and torques caused by the distal part. Subtracting these forces and torques from the measured forces and torques compensates the influence of the distal sensor part.

To identify the inertial parameters of the distal sensor part static identification was performed to estimate its mass m and center of mass coordinates $\vec{c} = (c_x, c_y, c_z)^T$ with respect to the sensor frame. Therefore the sensor was posed in different orientations. Before starting the identification procedure the sensor had been operating for three hours to achieve thermal stability and thus reducing drift. 100 orientations randomly drawn from an uniform, trivariate distribution of roll-pitch-yaw-angles parameterize the rotations of the sensor frame. In each sensor orientation, 1000 measurements were sampled and the sample mean was calculated in order to mitigate noise effects. Sensor drift effects were minimized by periodically resetting the sensor offsets in an initial pose after ten orientations had been approached. The batch least squares (LS) method [16] and the batch total least squares (TLS) method [17] were applied for identification. For this static method the gravity vector was determined through $\vec{g}_{init} = (0, 0, -g_0)^T$ with $g_0 = 9.80665 \frac{m}{s}^2$ in an initial pose. The respective gravity vector for each orientation, $\vec{g}$, was then calculated in order to identify m and $\vec{c}$. The corresponding simple equations are given by:

$$\begin{array}{rclcrcl} \vec{f}_{ij} & = & -m \cdot \vec{g} & \text{with} & i & = & 1 \ldots 1000 \text{ and} \\ \vec{\tau}_{ij} & = & -m \cdot \vec{c} \times \vec{g} & & j & = & 1 \ldots 100, \end{array}$$

where $\vec{f}_{ij}$ and $\vec{\tau}_{ij}$ represent the measured forces and torques. Using the setup described above, the parameter identification yielded the following mass properties of the distal sensor part of the JR3 sensor:

$$\begin{array}{rclcrcl} m & = & 56.4\,g & & c_y & = & 0.35\,mm \\ c_x & = & -1.65\,mm & & c_z & = & 10.3\,mm \end{array}$$

The results were obtained from experiments on two sensors by using the identification methods LS and TLS (note: $c_x \not\approx c_y$). The low mass of the distal sensor part and the compact geometric shape of the sensor suggest that the elements of the inertia matrix are negligible. Therefore dynamic identification was not performed and the elements of the inertia matrix are assumed to be zero. The essence here is that the mass of the distal part cannot be neglected when having light load masses mounted to the sensor. Independent from the manufacturer, this phenomenon is observed with any force/torque sensor.

D. Impulse Response and Crosstalk

For the purpose of inertial parameter estimation the impulse response of the sensor could influence the identification performance depending on its shape. In order to determine the approximate shape and duration of the f_z impulse response, the unloaded sensor was subjected to force impulses in z-direction. The impulses were generated by hitting the sensor with a plastic sphere of $0.12\,g$ mass that impacts on the sensor at the geometric center of its distal surface. After the impact it just bounces away again. The sensor was rigidly attached to a massive table with its proximal mounting surface, and the measured signals were sampled at the highest sampling rate of $8\,kSamples/s$. The duration, shape, and particularly the peak value of the impulse are unknown and thus merely admitting qualitative statements on the sensor impulse response.

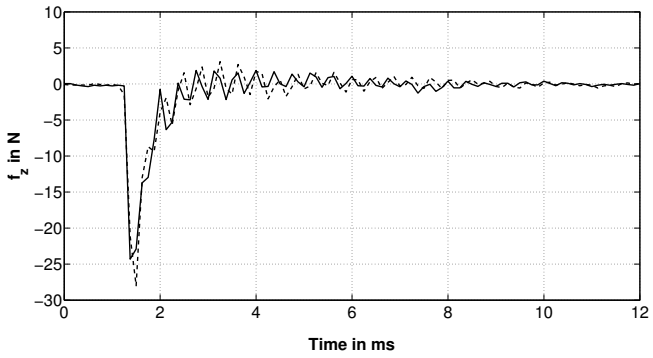

Fig. 5. Two *Impulse responses* of the force f_z after the impact of a plastic sphere.

The obtained impulse response of the force f_z shown in Fig. 5 is very short ($\approx 9\,ms$) and does only contain marginal oscillations after a short ($\approx 1\,ms$) initial negative peak. If the other force signals and torque signals show similar impulse responses, compensating the impulse response will probably not improve the performance. When a force impulse is applied in z-direction exactly in the geometric center of the sensor, ideally all measured signals except f_z are not influenced by the impulse. However, all force signals and all torque signals were influenced by the impulse. Since it could neither be guaranteed that the plastic sphere hits the sensor exactly in z-direction nor that it impinged exactly in its geometric center, disturbance forces and torques in other directions are probable. However, a force impulse in an arbitrary direction must *not* affect the linear acceleration and angular acceleration readings if the sensor does not move due to the impulse. In fact, both linear and angular acceleration signals show *substantial* disturbances caused by the applied force impulse although the sensor was immobilized by attaching it to a massive table. Additionally, the acceleration measurements during a trajectory execution suggest non-negligible sensitivity to vibrations perpendicular to the sensing axis of the accelerometers. These disturbances do not occur if the spectrum of the applied force concentrates at low frequencies, e.g. when a force of similar magnitude is applied manually. This observation suggests that the sensing elements indeed experience accelerations due to the impact.

Fig. 6 shows three linear acceleration measurements in z-direction showing the effects of the impacts. All three time-evolutions of the linear acceleration a_z show similar shapes. Note that the linear accelerations peak at $\approx 26\,m/s^2$ ($> 50\%$ of the full scale) and the influence of the impact lasts for approx. $20\,ms$ and thus leads to considerable adulteration of the measurements during this time. Fig. 7 depicts the angular

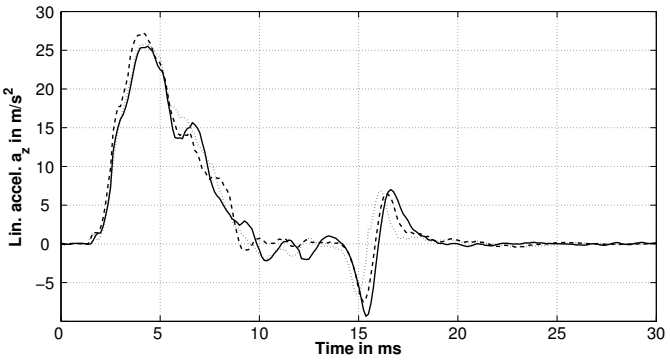

Fig. 6. Undesired effect of force impulses (cf. Fig. 5) in z-direction on the linear acceleration a_z shown by means of three sample responses.

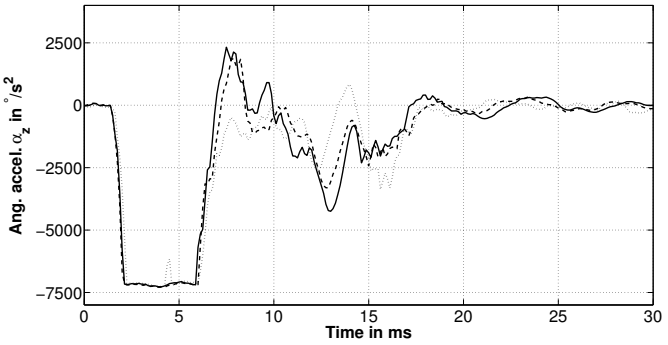

Fig. 7. Undesired effect of three different sample force impulses in z-direction on the angular acceleration α_z.

acceleration signals α_z of three trials in z-direction. Again, the signal shapes of the individual trials show considerable resemblance. The maximum angular acceleration of $\approx 5730^\circ/s^2$ is *clearly* exceeded by the measured angular acceleration in z-direction caused by the impact this maximum rating (Fig. 7).

Summarizing this Subsection leads to the awareness of substantial crosstalk between the different sensing elements for force/torque and acceleration. It is one of the major weaknesses as will be also pointed out in Section IV.

E. Noise

This part shortly summarizes experiments on noise analysis. In order to evaluate the noise characteristics, measurements of forces, torques and, accelerations were performed at three sampling rates using the unloaded sensor. Prior to data acquisition, the sensor had been operating for three hours in order to stabilize the sensor temperature and hence reduce temperature drift during the experiment.

Regarding the statistical characteristics experiments showed that the relative frequency distributions of the force and the torque noise amplitudes sampled at full sensor bandwidth, considerably differ from a Gaussian distribution whereas those of the linear and the angular acceleration noise amplitudes resemble Gaussian distributions.

The force signal of f_z shows an approx. three times higher noise variance than the f_x or the f_y signal. Note that the sensor maximum force ratings are twice as high in z-direction as in x-direction or y-direction. Thus this observation may be due to design differences in the foil strain gages for sensing f_z.

The acceleration signals show considerable noise *cross*-correlation, as already expected because of the employed acceleration sensing approach (cf. eqn. (1)–(6)). Knowledge of the cross-correlation may be beneficially employed in the design of Kalman filters for any preprocessing of $\vec{a}$ and $\vec{\alpha}$ by considering the cross-covariances of the measured signals in the measurement noise covariance matrix [18]. Regarding any preprocessing stage noise models of the linear and the angular acceleration noise may be incorporated into the Kalman filters, which may improve the performance in the presence of correlated noise.

Finally we can clearly state that systematic errors affecting all twelve signals contribute more to the total signal error than the noise. Therefore the implementation of noise models was not pursued; only the achievement of noise variances was employed to tune Kalman filters.

IV. Acceleration Signals Derived from Position Signals

Fig. 8a and Fig. 9a show linear and angular accelerations signals of the sensor frame's x-axis. The bold graph indicates the ideal/expected signal; it was theoretically calculated by considering all inertial parameters of a known test mass and all 18 position, velocity, and acceleration signals of a precalculated trajectory. The *real* acceleration signals are unknown, of course, and would be adulterated by unmodeled effects as material vibrations of the manipulator arm for instance. But another phenomenon shows that these unmodeled effects only cause small and negligible additional magnitudes. Force and torque signals, which are only excited by the inertia of a sample mass during a test trajectory, match exactly with the theoretically calculated ones. This fact lets us assume that the bold line is very close the real acceleration signal.

The second signal in Figs. 8a and 9a was recorded during the execution of a jerk-limited, sinusoidal shaped trajectory on a Stäubli RX60 industrial manipulator. As one can see in Fig. 9a the α_x signal exhibits strong disturbances and already exceeds the maximum values of the sensor even though a very soft and not too dynamic trajectory was chosen.

Due to the bad characteristics of all three angular acceleration signals, actually these signals did not lead to any successful experiments, the idea of deriving the angular acceleration vector $\vec{\alpha}$ from position measurements was born and is supposed to be commented in this Section.

Joint angle measurements $\vec{q}(t)$ are used to derive the angular velocity vector $\vec{\omega}(t)$ as well as an alternative representation of the angular acceleration vector $\vec{\alpha}(t)$ with respect to the sensor frame. Hence the differentiation or double differentiation, respectively, of the joint angle measurements is necessary. Unfortunately differentiation using forward, backward, or central difference operators, increases the noise contained in the signal. The most promising results were achieved with

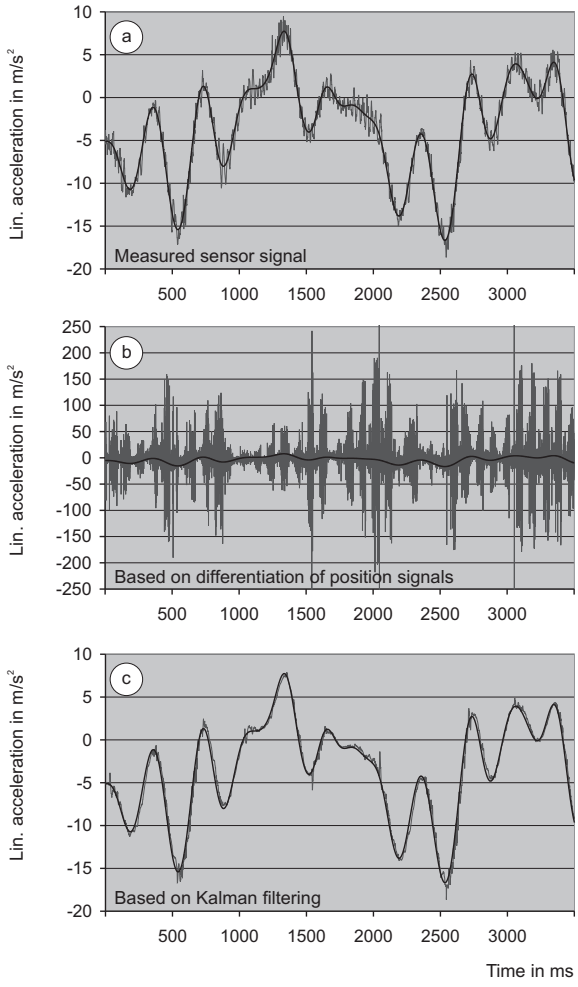

Fig. 8. Linear acceleration of the manipulator sensor frame's x-axis a_x: a) directly measured sensor values, b) based on differentiation (eqn. 7), and c) based on Kalman filtering The bold line indicates the evolution of the ideal signal.

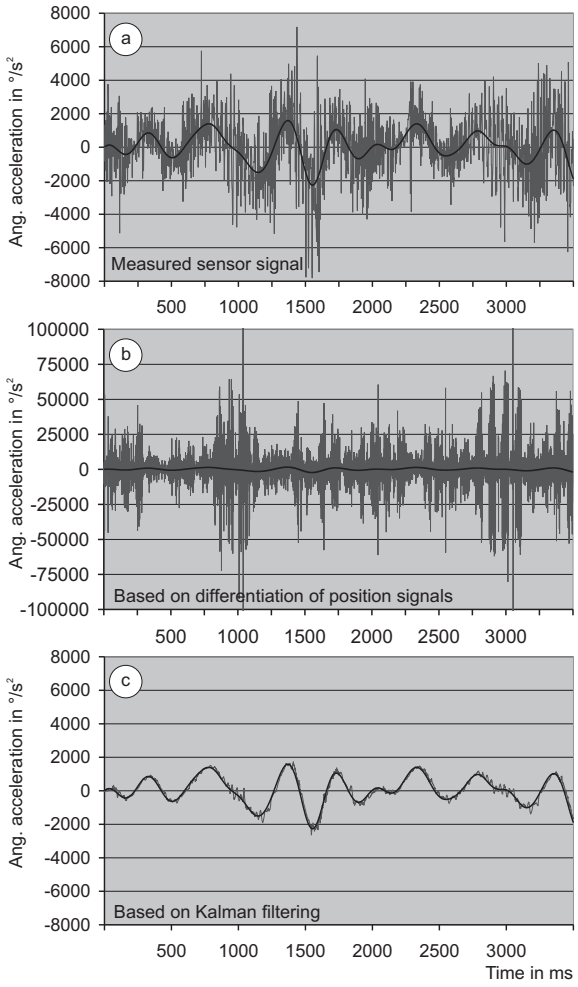

Fig. 9. Analogon to Fig. 8 for angular accelerations: a) directly measured values of α_x, b) based on differentiation of position signals, and c) based on Kalman filtering. The bold line indicates the ideal signal again.

the central difference operator. Although the joint angle signals $\vec{q}(t)$ are not remarkably affected by noise, the angular velocity signals $\dot{\vec{q}}(t)$ obtained by differentiating the joint angle signals show considerable noise. Disturbances contained in the individual joint angle measurements and the derived joint angular velocities and joint angular accelerations $\ddot{\vec{q}}(t)$ are also propagated through the kinematic chain. Thus parameters expressed with respect to the sensor frame are influenced by disturbances originating from all six joints. This error propagation problem is even intensified by the high non-linearity of the transformation matrices with respect to the joint angles. If the joint variables, obtained by differentiation, are used to derive the acceleration vectors $\vec{a}$ and $\vec{\alpha}$ with respect to the sensor frame, these elements of the vector are clearly dominated by noise as Figs. 8b and 9b depict exemplarily. These signals were obtained after a double differentiation by

$$\ddot{q}_k(t) = \frac{q_k(t+\Delta t) - 2q_k(t) + q_k(t-\Delta t)}{(\Delta t)^2} \qquad (7)$$

in joint space followed by a transformation into the sensor frame (please note the different scalings in Figs. 8 and 9). Simple FIR/IIR post-filtering indeed results in a lower noise level but the group delay of the filter delays the filtered signal. This, in turn, may not be acceptable when heading for instance for identification algorithms based on these signals. Moreover the filter characteristics, particularly the cut-off frequency, have to be adapted to the bandwidth of the input signal in order to minimize the noise level. Ovaska [19] surveyed several approaches to angular acceleration measurement in the presence of noise. Regarding indirect acceleration measurements two major approaches can be distinguished. The first approach uses a differentiator followed by a low-pass filter. In order to eliminate the group delay of standard FIR/IIR filters, predictive filters may be employed. One weak point of this approach is the necessity to optimize the cut-off frequency of the filter depending on the maximum signal frequency in order to guarantee best-possible noise suppression regardless of the executed trajectory. Furthermore, the applicability of

this approach is constrained since velocity or acceleration signals that cannot be accurately approximated by low-order polynomials deteriorate its performance [19].

The second approach is based on linear state observation using Kalman-filtering techniques. In contrast to the first approach, it is not limited to a certain class of signals. As a linear Kalman filter is additionally inexpensive concerning its computational complexity and easy to implement, the latter approach is favored. The derivation of the joint angular velocity and the joint angular acceleration is described by a linear state space model, affected by additive Gaussian noise, whose characteristics influence the filter behavior.

A variant of the Kalman filter, used to derive both joint angular velocity $\dot{\vec{q}}(t)$ and joint angular acceleration $\ddot{\vec{q}}(t)$ from joint angle measurements $\vec{q}(t)$, uses the linear continuous state-space model and was proposed by Bélanger [20]. This state-space model estimates a state, which incorporates the joint angular velocity $\dot{q}_k(t)$, the joint angular acceleration $\ddot{q}_k(t)$, and the joint angle $q_k(t)$ itself, for each joint k.

Based on the approaches from [19] and [20] the filtered joint angles, angular velocities, and angular accelerations are used to derive motion parameters with respect to the sensor frame. The Figs. 8c and 9c exemplarily show the Kalman filtered signals $a_x(t)$ and $\alpha_x(t)$ based on measured joint angle signals $\vec{q}(t)$. In contrast to the Kalman filter-based signal, the measured angular acceleration signal is dominated by disturbances.

The quintessence of this section is that especially the angular accelerations can be obtained in sufficient quality by using measured joint position signals and Kalman filter techniques, while the directly measured angular accelerations exhibit strong disturbances. The fact that a complete set of acceleration signals measured in a typical setup with respect to a frame fixed to the end-effector of a robotic manipulator can be achieved without additional sensing, is supposed to be really promising and valuable.

V. Summary and Conclusions

This paper summarizes experiences with force/torque and acceleration measurements in six axes. The aim was to fuse all twelve signals in order to enable the estimation of inertial parameters, to improve control behavior, to recognize objects, to gain force control performance, or to make visual-servoing methods more robust. The geometric arrangement of typical accelerometers as the twelve-DOF sensor of JR3 was explained. Systematic errors, which naturally occur during the usage of six-axis force/torque sensors together with six-axis accelerometers, were derived and discussed.

The major contribution of this paper however is, that the signal characteristics of typical sensor setups are analyzed and characterized with the essential result, that strongly disturbed measured acceleration signals, especially angular acceleration signals, can be sufficiently replaced by Kalman filter based signals derived from joint position measurements. These signals can sufficiently be fused with measured force/torque signals.

As second major conclusion we state that the methods of Ovaska et al. [19] and Belanger et al. [20] to derive acceleration information from joint position measurements deliver excellent results – herewith we clearly confirm the results of these techniques.

Institutions that consider buying a twelve-DOF sensor might think about this methodology and decide to achieve acceleration values from Kalman-filtered position signals. Sophistications might appear only if the manipulator acts on a mobile platform, such that accelerations of the platform itself can not be neglected when regarding forces and torques caused by inertia. This is an issue that has not been addressed in this paper, and which is part of our future work: the investigation of force/torque and acceleration sensor data fusion on robotic manipulation arms, whose bases are non-fixed and also influenced by further accelerations, e.g. arms on mobile platforms. Research and development institutions that are heading for acceleration sensing integration in these kinds of systems are always welcome to share the authors experiences on this technology.

Institutions that already own or use a comparable setup of six-DOF accelerometers should also profit from the reported experiences, of course.

As stated in the introduction, only a few works have been done on these technologies yet, but the potential is really high for a wide bandwidth of robotic applications. The authors would like to encourage developers and researchers to take a closer look on methods using twelve-axis force/torque and acceleration information and their potential – we are just beginning to explore new applications using the potential of this wide field.

Acknowledgment

The authors would like to thank *QNX Software Systems* for providing free software licenses.

References

[1] T. Kröger, D. Kubus, and F. M. Wahl. Force and acceleration sensor fusion for compliant manipulation control in six degrees of freedom. *Accepted for Publishing in: Advanced Robotics, Special Issue on Selected Papers from IROS 2006*, November 2007.

[2] D. Kubus, T. Kröger, and F. M. Wahl. On-line rigid object recognition and pose estimation based on inertial parameters. *Accepted for Publishing at IEEE International Conference on Intelligent Robots and Systems*, October 2007.

[3] R. Smits, H. Bruyninckx, J. Baeten, P. Slaets, and J. De Schutter. Model based position-force-vision sensor fusion for robot compliant motion control. In *Proc. of IEEE International Conference on Multisensor Fusion and Integration for Intelligent Systems*, pages 501–506, September 2006.

[4] J. Gámez García, A. Robertsson, J. Gómez Ortega, and R. Johansson. Sensor fusion of force and acceleration for robot force control. In *Proc. of IEEE/RSJ International Conference on Intellegent Robotic Systems*, pages 3009–3014, 2004.

[5] J. Gámez García, A. Robertsson, J. Gómez Ortega, and R. Johansson. Generalized contact force estimator for a robot manipulator. In *Proc. of IEEE International Conference on Robotics and Automation*, pages 4019–4024, 2006.

[6] T. Kröger, D. Kubus, and F. M. Wahl. 6D force and acceleration sensor fusion for compliant manipulation control. In *Proc. of IEEE/RSJ International Conference on Intellegent Robotic Systems*, pages 2626–2631, 2006.

[7] Z. Wu, M. Meng, and F. Shen. Interaction force measurement of robotic manipulator based on 12dof force sensor. In *International Conference on Information Aquisition*, pages 240–243, 2004.

[8] M. Meng, Z. Wu, Y. Yu, Y. Ge, and Y. Ge. Design and characterization of a six-axis accelerometer. In *Proc. of IEEE International Conference on Robotics and Automation*, pages 2367–2372, 2005.

[9] R. Puers and S. Reyntjens. Design and processing experiments of a new miniaturized capacitive triaxial accelerometer. *Sensors and Actuators A: Physical*, 68(1–3):324–328, June 1998.

[10] R. Amarasinghe, D. V. Dao, T. Toriyama, and S. Sugiyama. Development of miniaturized 6-axis accelerometer utilizing piezoresistive sensing elements. *Sensors and Actuators A: Physical*, 134(2):310–320, March 2007.

[11] K. Kunz, P. Enoksson, and G. Stemme. Highly sensitive triaxial silicon accelerometer with integrated pzt thin film detectors. *Sensors and Actuators A: Physical*, 92(1–3):156–160, August 2001.

[12] V. Chapsky, V. T. Portmana, and B.-Z. Sandlera. Single-mass 6-dof isotropic accelerometer with segmented psd sensors. *Sensors and Actuators A: Physical*, 135(2):558–569, April 2007.

[13] J. Bryzek, S. Roundy, B. Bircumshaw, C. Chung, K. Castellino, J. R. Stetter, and M. Vestel. Marvelous mems – advanced ic sensors and microstructures for high volume applications. *IEEE Circuits and Devices Magazine*, 17(8):8–28, March 2006.

[14] K.-J. Xu and C. Li. Dynamic decoupling and compensating methods of multi-axis force sensors. *IEEE Trans. on Instrumentation and Measurement*, 49(5):935–941, 2000.

[15] J. Ramming. JR3 inc. homepage. ⟨http://www.jr3.com⟩ [date: 07/30/2007]. Internet, 2007.

[16] L. Ljung. *System Identification: Theory for the User*. Prentice Hall, 1999.

[17] S. Van Huffel and J. Vandewalle. *The Total Least Squares Problem: Computational Aspects and Analysis*, volume 9 of *Frontiers in Applied Mathematics*. SIAM, 1992.

[18] A. V. Oppenheim and R. W. Schafer. *Discrete-Time Signal Processing*. Prentice Hall Signal Processing Series. Prentice Hall, 1999.

[19] S. J. Ovaska and S. Valiviita. Angular acceleration measurement: A review. *IEEE Trans. on Instrumentation and Measurement*, 47(5):1211–1217, October 1998.

[20] P. R. Bélanger, P. Dobrovolny, A. Helmy, and X. Zhang. Estimation of angular velocity and acceleration from shaft-encoder measurements. *The International Journal of Robotics Research*, 17(11):1225–1233, 1998.